Science of Sintering, **52** (2020) 257-268

doi:https://doi.org/10.2298/SOS2003257F

UDK: 553.689; 666.651; 535.375

Structure and Properties of Nanocrystalline Tetragonal $BaTiO_3$ Prepared by Combustion Solid State Synthesis

S. Filipović[1*)], Lj. Anđelković[2], D. Jeremić[3], P. Vulić[4], A. S. Nikolić[5], S. Marković[1], V. Paunović[6], S. Lević[7], V. B. Pavlović[7]

[1]Institute of Technical Sciences of SASA, Knez Mihailova 35/IV, 11000 Belgrade, Serbia

[2]University of Belgrade, Institute of Chemistry, Technology and Metallurgy, Department of Chemistry, Njegoševa 12, 11000 Belgrade, Serbia

[3]Innovation Center of the Faculty of Chemistry, University of Belgrade, Studentski trg 12-16, 11158 Belgrade, Serbia

[4]University of Belgrade, Faculty of Mining and Geology, Đušina 7, 11000 Belgrade, Serbia

[5]University of Belgrade, Faculty of Chemistry, Studentski trg 12-16, 11158 Belgrade, Serbia

[6]University of Niš, Faculty of Electronic Engineering, Aleksandra Medvedeva 14, 18000 Niš, Serbia

[7]University of Belgrade, Faculty of Agriculture, Nemanjina 6, 11080 Belgrade, Serbia

Abstract:

Barium titanate ($BaTiO_3$) attracts high scientific and technological attention due to good dielectric and electromechanical properties. Although $BaTiO_3$ is one of the most frequently investigated ferroelectric materials, the need for finding new and/or improved synthesis methods of this material still exists. In this paper, a novel, mild synthesis route for producing tetragonal $BaTiO_3$ from barium nitrate and Ti-oxalate precursor is presented. Morphology of the prepared and subsequently sintered $BaTiO_3$ was determined by SEM. Particle size distribution of the as prepared powder was monitored by the laser diffraction. The phase composition, structure and lattice dynamics were investigated by XRD and Raman spectroscopy. Finally, dielectric parameters were determined in the temperature range from 30 to 180 ^oC, and within a variety of frequencies. Curie temperature was detected at 130 ^oC.

Keywords*: Nanocrystaline $BaTiO_3$; Combustion synthesis; XRD; Raman spectroscopy; Dielectric properties.*

1. Introduction

Materials based on perovskite structure have found a variety of applications in electronics due to their ferroelectric properties [1, 2]. Among them, one of the most investigated is barium titanate ($BaTiO_3$). This ferroelastic and ferroelectric ceramic material has been used for multilayer ceramic capacitors (MLCC), positive temperature coefficient thermistors, and electro-optic devices, due to its high dielectric constant [3, 4]. Furthermore, interest in investigating lead-free ferroelectric ceramics is rising because of environmental concern. Here $BaTiO_3$ finds its opportunity [5].

*) **Corresponding author:** suzana.filipović@itn.sanu.ac.rs

With an increase of temperature, $BaTiO_3$ undergoes a few phase transitions: rhombohedral→orthorhombic→tetragonal→cubic [6]. Some of the properties of cubic and tetragonal $BaTiO_3$ are diametrically different, since cubic $BaTiO_3$ is paraelectric, while tetragonal $BaTiO_3$ is ferroelectric.

Till today, various techniques have been used for the preparation of tetragonal $BaTiO_3$, sonochemical synthesis, sol-gel, hydrothermal, solvothermal, chemical co-precipitation, mechanochemical, supercritical fluid, etc [7, 8]. Solid-state synthesis, followed by calcination at above 1000 °C, presents one of the most cost-effective methods for the preparation of $BaTiO_3$ at mass scale. However, the reactions at such high temperatures are almost impossible to control and the obtained powders often have large particle size and wide particle size distribution. The literature data indicate that solid-state synthesis from $BaCO_3$ and TiO_2 was used the most frequently [9-11]. The pure $BaTiO_3$ was dominantly produced by this reaction, but with irregular structure and the presence of large agglomerates. Microstructure could be slightly improved by using mechanical treatment, but problem of agglomeration remains along with increasing microstrain [12]. Contrarily, as the particle size decreases to the nano-level aggregation becomes a significant drawback. It has been shown that reaction for the fabrication of the barium titanate from $Ba(NO_3)_2$ and TiO_2 is promising, because the reaction occurs through liquid-solid phase reaction, which decreases requested temperature [13]. Furthermore, it was demonstrated that the presence of reducing agent in system $Ba(NO_3)_2$ -TiO_2 lowers energy consumption during preparation [2]. On the other hand, the synthesis of $BaTiO_3$ from oxalates often includes a complicated procedure with dissolving either barium oxalate or titanium oxalate in water or alcohols and subsequent precipitation under low pH, calcinations, etc [14-16]. So, the search for an improved method for the fabrication of $BaTiO_3$ still exists. Generally, when considering techniques to synthesize barium titanate, ideally they should require minimal steps and mild conditions.

In this paper, we sought to reveal a new approach of producing nanocrystalline tetragonal barium titanate powder based on combustion method. The synthesized $[Ti_2O_3(H_2O)_2](C_2O_4)\cdot H_2O$ and the commercial barium nitrate was used to develop an alternative low-temperature method for the preparation of crystalline $BaTiO_3$ powders at low cost. Unlike other titanium compounds, such as lactates, the oxalate complex has optimal content of carbon, enabling fast and easy reaction with barium nitrate at lower temperatures. The comprehensive characterization, including investigation of dielectric properties, of thus prepared powder was performed.

2. Materials and Experimental Procedures

Synthesis procedure was started by the preparation of Ti precursor. Titanium (IV) oxalate $[Ti_2O_3(H_2O)_2](C_2O_4)\cdot H_2O$ was prepared by the procedure described by Boudaren et al. in [17]. Mixture of 1 g (3.49 mmol) of synthesized titanium (IV) oxalate and 0.46 g (1.76 mmol) of commercial p.a. barium nitrate was pulverized in an agate mortar and wetted with methanol to make a homogenous paste. The paste was burned on a Bunsen burner for a 30 min at around 650 °C (measured within the reaction vessel with infrared thermometer). Produced solid was further thermally processed in an electric furnace for 2 h at 700 °C.

XRD patterns of Ti precursor and synthesized sample, were collected using a Rigaku SmartLab automated powder X-ray diffractometer with Cu $K\alpha_{1,2}$ (λ = 1.54059 Å) radiation (U = 40 kV, I = 30 mA) equipped with D/teX Ultra 250 stripped 1D detector in the standard mode. The diffraction angle range was 5–75 °2θ for Ti precursor, while for the synthesized $BaTiO_3$ it was 10–90 °2θ, with a step of 0.01° at a scan speed of 2 °/min.

Morphology of prepared sample was investigated by SEM. SEM images of powder and sintered sample were taken with a JEOL JSM-6610LV scanning electron microscope. The powder and crushed sintered sample were coated with gold to minimize charging.

Particle size distribution was examined by the laser diffraction on Mastersizer 2000 Malvern Instruments Ltd. The used instrument covers the particle size range of 0.02-2000 μm. For experiment's purpose the powder was dispersed in distilled water. Particle size distribution of obtained dispersion was recorded as it is. Dispersion was subjected to low-intensity ultrasound irradiation (US), at a frequency of 40 kHz and power of 50 W for 5 minutes, and distribution was measured again.

The powder was compacted at 300 MPa using a uniaxial double action pressing process with an 8 mm diameter tool, hydraulic press RING, P-14, VEB THURINGER. Dilatometric curve was obtained by SETSYS Evolution TMA, Setaram Instrumentation, in temperature range from 25 to 1200 ^{o}C, with heating rate of 10 ^{o}C·min^{-1}, and dwell time at the highest temperature for 2h. Measurement was performed in air atmosphere.

Raman spectra were collected with a XploRA Raman spectrometer Horiba Jobin Yvon. The system uses a laser at 532 nm, with power of 0.25 MW at the sample. The spectrum was recorded in the range of 100-1400 cm^{-1}, using the spectrometer equipped with a 2400 lines/mm grating.

Electrical characteristics were measured using Agilent 4284A precision LCR meter in frequency range from 0.2 kHz to 1 MHz. Measurements were performed in temperature interval from 30 to 180 ^{o}C, in temperature chamber Heraeus HEP2, which is fully automated. Prior to electrical measurements, silver paste was applied on flat surfaces of specimens.

3. Results and Discussion

The obtained XRD results were analyzed by the Rietveld method to gain deeper insight into the structural and microstructural parameters. The fundamental parameters approach [18] was implemented in PDXL2 Rigaku software.

The powder XRD patterns for synthesized precursor and $BaTiO_3$ containing powder are shown in Fig. 1. The d-values and intensities of the diffraction maxima match the literature data of $C_2H_2O_4{\cdot}H_2O$ (ICDD PDF 78-6680) and $[Ti_2O_3(H_2O)_2](C_2O_4){\cdot}H_2O$ (ICDD PDF 74-3385) for Ti precursor. In the synthesized powder $BaTiO_3$ (65 %, ICDD PDF 79-2265), $BaCO_3$ (23 %, ICDD PDF 83-3088) and TiO_2 (12 %, ICDD PDF 70-7348) crystalline phases were detected. It is important to notice that the X-ray diffraction pattern (Fig. 1b) shows broad peaks indicating the ultrafine nature and small crystallite size of the $BaTiO_3$. It should be additionally emphasized that synthesized barium titanate has average crystallite size 36 nm and tetragonal structure, based on data obtained from Rietveld refinement, as presented in Table I. This is even more important having in mind that grain size effects have significant influence on phase transition in $BaTiO_3$. It has been shown, that various causes (internal stresses, absence of long-range cooperative interaction, etc.) can lead to transition tetragonal $BaTiO_3$ into cubic with decreasing crystallite size [20]. The critical size, where the grain size effect occures is in the range 20 to 100 nm, and stronglly depends on preparation method [20]. Among other methods, mechanicall activation can be used for obtaining nanocrystalline $BaTiO_3$ with tetragonal symetry. But, occurrence of the microstrain higher than 0.5 % and the unstable phonon states diminishes possibilities of use of the mechanical activation for production of the tetragonal, nano-sized $BaTiO_3$ [21].

The particle size distribution of the synthesized powder (Fig. 2a) shows the polimodal distribution. The small particles (less than 1μm) were associated in agglomerates with average size around 22 μm. Agglomerates bigger than 100 μm were also noticed. This association is the consequence of heating during the synthesis of $BaTiO_3$. After short treatment (5 min) in an ultrasound bath (Fig. 2b), distribution was shifted to the left. Mild US irradiation decreases all characteristic values (d(0,1), d(0,5) and d(0,9)), breaks down particles aggregations and slightly reduces width of the distribution. A measured value of the *span*, which is below 3 (2.931 and 2.837, before and after US, respectively) indicates relatively narrow distribution.

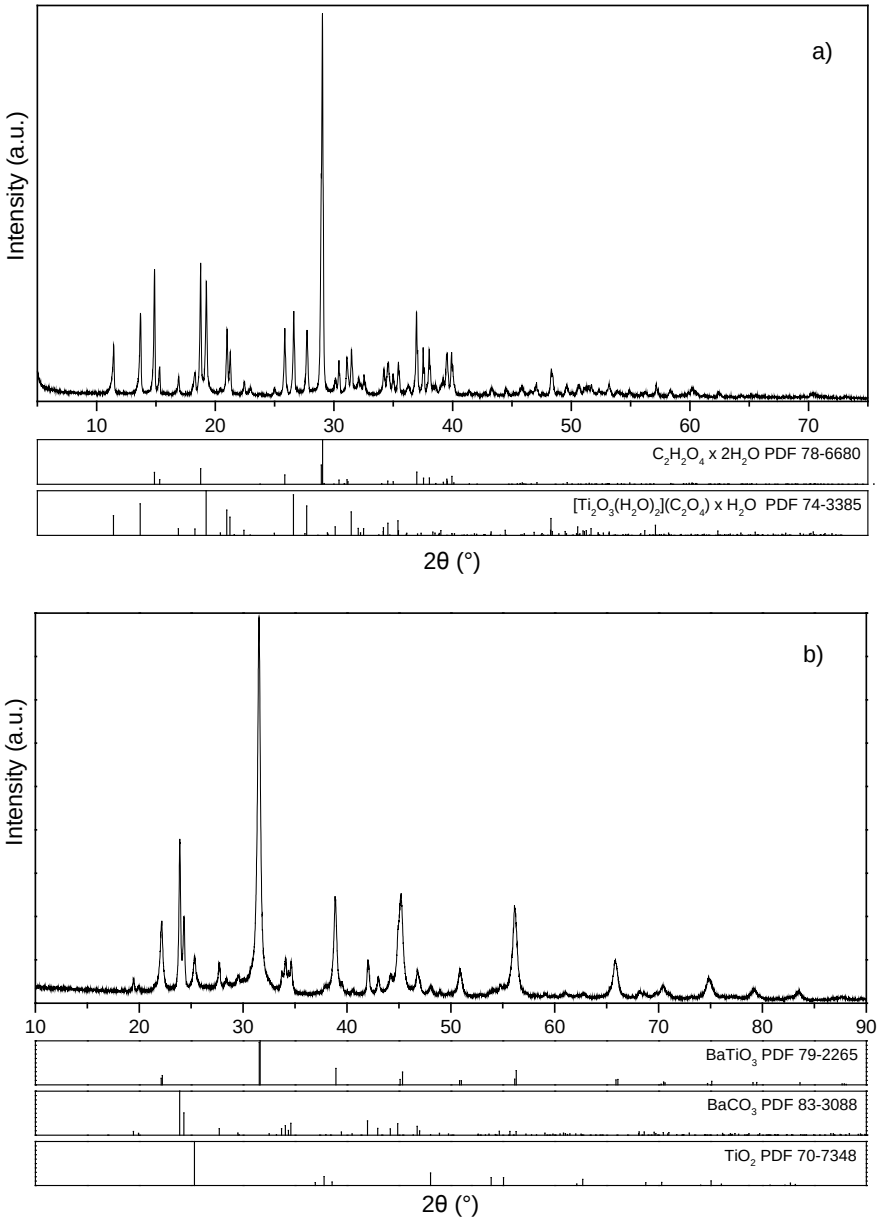

Fig.1. Colected XRD data for Ti precursor (a) and the synthesized powder (b).

Tab. I Unit cell and microstructural parameters for Ti precursor and the synthesized crystalline phases.

Phase	***a* (Å)**	***b* (Å)**	***c* (Å)**	**Volume ($Å^3$)**	**Crystallite Size (nm)**	**Microstrain (%)**
Ti precursor	15.4863(9)	10.4819(6)	9.6939(6)	1573.6(2)	132(4)	0.00(2)
$BaTiO_3$	4.0007(9)	4.0007(9)	4.0186(8)	64.32(2)	36(1)	0.26(1)
$BaCO_3$	5.3080(3)	8.9026(6)	6.4428(4)	304.46(3)	653(12)	0.30(2)
TiO_2	3.7838(5)	3.7838(5)	9.4786(13)	135.71(4)	109(10)	0.53(2)

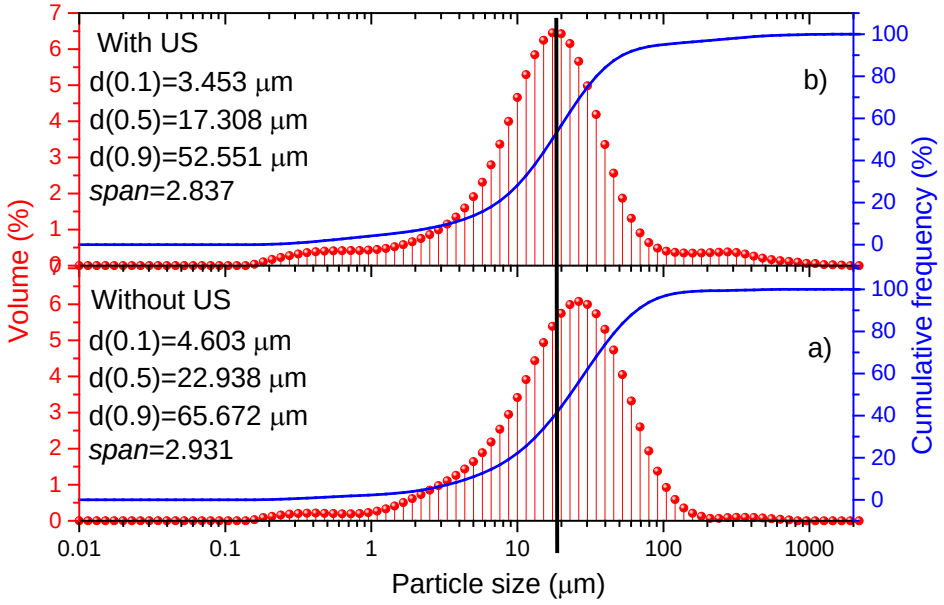

Fig. 2. Particle size distribution of a) the as synthesized powder b) the powder after applied ultrasound treatment.

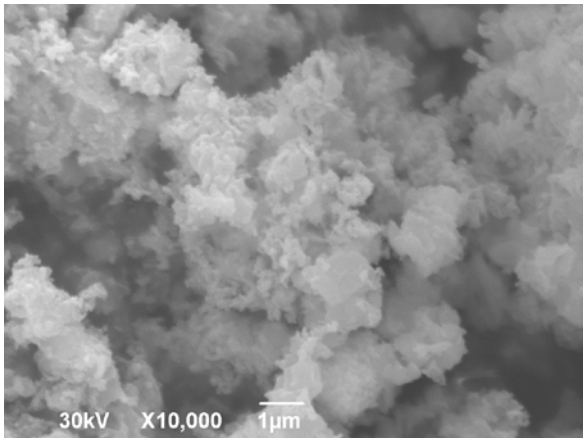

Fig. 3. SEM micrograph of $BaTiO_3$ powder.

The micrograph of the synthesized powder that contains $BaTiO_3$ is presented in Fig. 3. Two different kinds of particles are noticed. Larger particles are of polygonal shape, approximately 2-3 μm in length, while smaller ones are spherical. The larger correspond to $BaCO_3$, as confirmed with XRD results. The spherical particles are ranged from 200 to 500 nm in diameter. They are composed from $BaTiO_3$ and a smaller amount of TiO_2 particles, which is in good agreement with XRD analysis. Finer grains have a tendency to associate in aggregation. Heat treatment at 700 ^oC has led to an increase in the particle size. Bigger agglomerates are hard and cannot be crushed in the ultrasound bath, which was shown by analyzing particle size distribution (Fig. 2.).

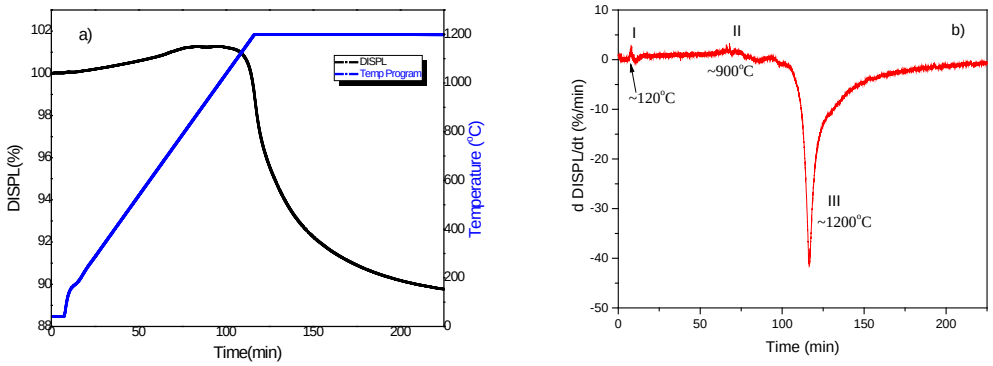

Fig. 4. Dilatometric curve of as synthesized $BaTiO_3$.

Sintering of pressed sample was performed in high-resolution TMA. Shrinkage curve of the specimen with applied temperature program in the dilatometer is presented in Fig. 4a. With increasing temperature, thermal expansion can be clearly noticed through the non-isothermal stadium. Shrinking occurs slightly before beginning of the isothermal heating regime. The onset of sintering is detected at around 1120 ^oC. Total detected shrinkage of the sample is about 11 %. The extensive look of the dilatometric curve, in the isothermal regime, indicates that two processes occur simultaneously. It can be noticed that the sintering and the recrystallization take place at the same time. The differential curve, presented in the Fig. 4b, shows more clearly temperatures of processes that are happening during heating. Phase transition from the tetragonal to the cubic phase of $BaTiO_3$ occurs approximately at 120 ^oC. This transition is typical for the $BaTiO_3$ [22-24]. The second phase transition is detected in temperature region from 760 to 950 ^oC. This event originates from the anatase to the rutile phase transformation. It is known that this phase transition undergoes gradually in the temperature range 500-1200 ^oC, and is strongly related to size and surface effects of the titanium dioxide [25-29]. Besides, phase transition of the $BaCO_3$ is also possible in this region [29]. It should be mentioned that the $BaCO_3$ is the most common secondary phase formed during the $BaTiO_3$ powder preparation by any synthesis route [13]. Phase transition of the α-$BaCO_3$ into the β-$BaCO_3$ occurs at 800 ^oC with an increase in molar volume by 2.7 %. Taking into account the results obtained from XRD, both processes can be responsible for these changes in the region marked with II in the Fig. 4b. The highest shrinkage rate occurs at 1200 ^oC, at the moment when isothermal sintering starts. Based on available literature data, maximum shrinkage rate, for the un-doped barium titanate, occurs above 1250 ^oC [30, 31]. The presence of the additives can shift the temperature of the maximum shrinkage rate (T_{MSR}) to the lower [31]. In our case, the shifting of T_{MSR} can be explained by the presence of carbonates.

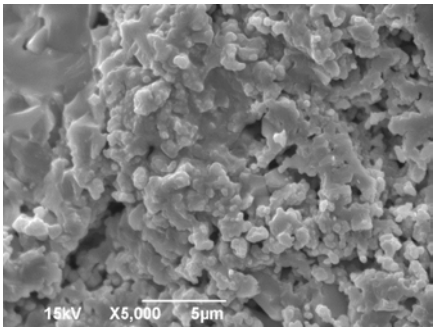

Fig. 5. SEM of the $BaTiO_3$ sample sintered in dilatometer.

SEM micrograph of the sintered sample is presented in Fig. 5. It is noticeable that the sample is in the medium sintering stage. High open porosity is detected along with randomized closed pores with the irregular shape of edges. Well-sintered areas are also presented, while the largest share of particles retains their individuality. The sintered sample reached 70 % of TD, calculated by measuring mass and dimensions of the sintered specimen.

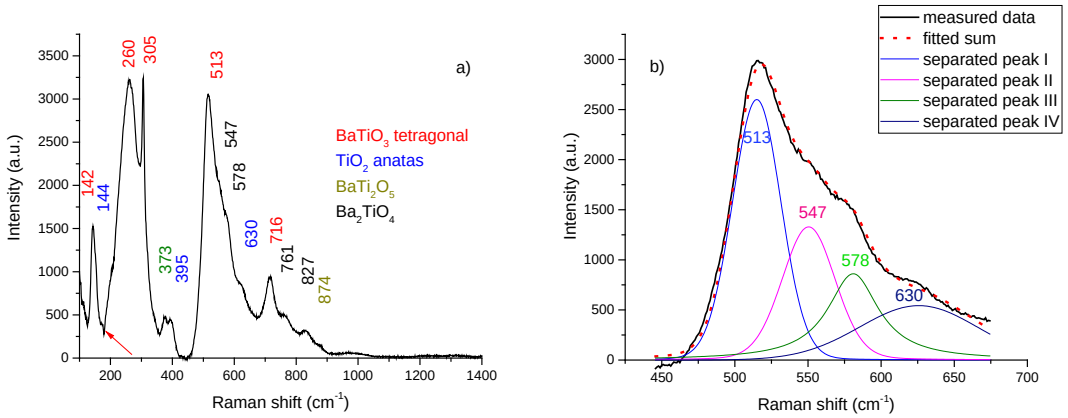

Fig. 6. Raman spectra of the sintered $BaTiO_3$ sample (a), deconvoluted segment between 450 and 670 cm^{-1} (b).

Raman spectrum of the sintered sample was presented in Fig. 6. Appearance of the sharp and narrow picks points out long-range ordered crystal structure. By symmetry, tetragonal $BaTiO_3$ has 10 Raman active modes. Dominant characteristic of tetragonal structure in the Raman spectra of $BaTiO_3$ are modes at 306 cm^{-1} (E(LO + TO), B_1) and 716 cm^{-1} (E(LO), $A1$(LO)) [32-34]. These characteristic modes are detected in Raman spectra of the sintered sample (Fig. 6a). Besides them, other reflections, that originate from the tetragonal phase of barium titanate (146, 260, 513 cm^{-1}), were present. The negative intensity peak at 180 cm^{-1}, marked with red arrow in Fig. 6a, is characteristic of powder samples with sub-micron crystallite size [35]. This is the result of the interference between Raman-scattered radiations from two different modes, as it was proposed by Frey and Payne [19]. The modes of the anatase [36] were also present in the spectra, along with weak modes of intermediary phases $BaTi_2O_5$ and Ba_2TiO_4 [37]. The wide and asymmetric mode in the range of 450 to 670 cm^{-1} was additionally fitted in order to determine the exact positions of four overleaped modes (Fig. 6b). Deconvolution was performed in the sum of separated peaks, using PeakFit™ software [38].

Synthesis of barium titanate from $Ba(NO_3)_2$ and TiO_2 was followed by the formation of a notable amount of the $BaCO_3$ [2]. It is known that the reaction between $BaCO_3$ and titanium dioxide goes through several steps involving $BaTi_2O_5$, Ba_2TiO_4, and other barium titanate intermediary compounds. This reaction occurs at the surface of the $BaCO_3$ grains and the dominant driving force for it is the diffusion process [39]. The existence of intermediate barium titanate phases and anatase in Raman spectra of sintered sample indicates that reaction isn't completed. Modes of the $BaCO_3$ aren't detected. This is because Raman provides more local images giving information about the thin surface layer of the sample. The $BaCO_3$ can be located inside of the aggregates covered by one of the intermediate phases, and hence cannot be detected by Raman spectroscopy.

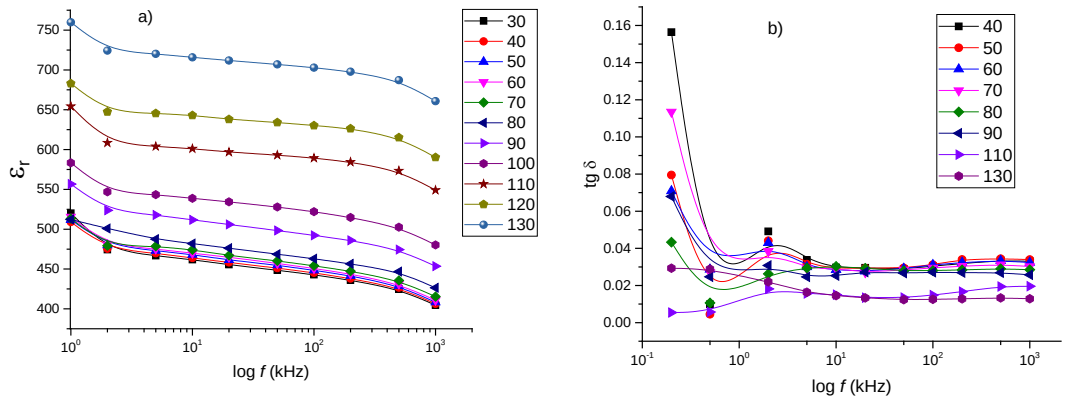

Fig. 7. Real part of the complex dielectric permittivity (a) and tgδ (b) vs. frequency measured in temperature range 30-130 °C.

The real part of complex dielectric permittivity measured at different temperatures is presenred in Fig. 7a. The main characteristic of these graphics is that ε_r decreases at lower frequencies and remains almost constant at higher frequencies. This behavior is common for many dielectric materials [40, 41]. Having in mind that the permittivity is a parameter connected with the polarization and that with higher applied frequencies less types of the polarization can be accomplished, reduction in ε_r with f is clear [23, 42].

Drastic decrease vs. frequency was measured for the dissipation factor (Fig. 7b). The diagram clearly exhibits two regions. The first one can be noticed below 1 kHz where the slop is the steepest, while the second region occurs between 1 kHz and 1 MHz, where the loss tangent remains constant with increasing frequency. The loss tangent takes values from 0.03 to 0.01 for observed temperature range.

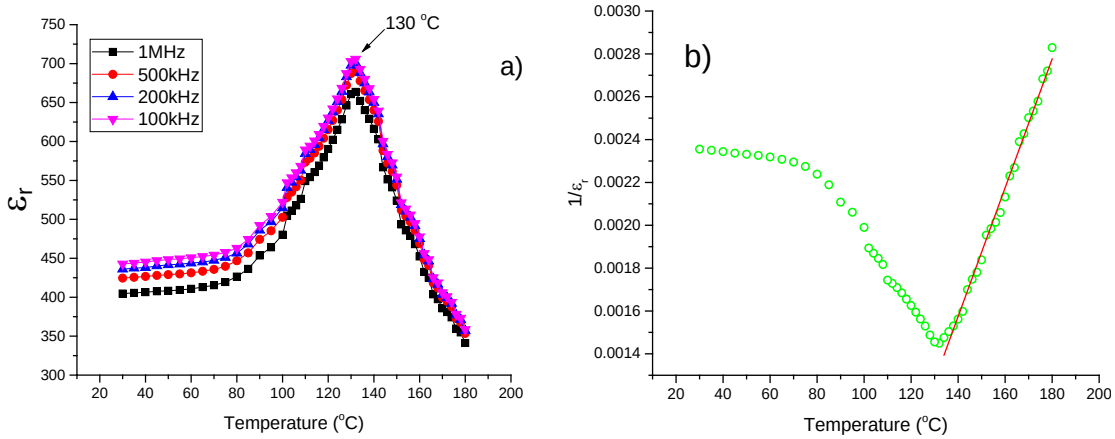

Fig. 8. Change in the real part of the complex dielectric permittivity (a) and reciprocal value of ε_r (b)with temperature.

Temperature dependence of ε_r at four selected frequencies is presented in Fig. 8a. Sharp pick at 130 °C occurs for all frequencies. This pick is related with the tetragonal (ferroelectric)–cubic (paraelectric) phase transition within the $BaTiO_3$. Obtained Curie temperature is very close to the theoretical value for $BaTiO_3$ [43-45]. It has been shown that

the presence of defects and microstrain within the lattice, leads to an increase of free energy inside, so less energy is necessary for phase transition and T_c shifts toward lower [46]. Appearance of T_c at 130 ^oC implies a highly ordered crystal structure.

Relatively low dielectric permittivity can be attributed to the low achieved density, the presence of open porosity, inhomogeneous morphology and non-uniform grains distribution. Furthermore, the presence of secondary phases can be responsible for a decrease in dielectric constant [47].

In addition, Curie-Weiss low (Eq. 1) is applied to the results obtained at 500 kHz to calculate the dielectric parameters such as the Curie constant (C) and the Curie-Weiss temperature (T_0).

$$\varepsilon_r = \frac{C}{T - T_0} \qquad (1)$$

The C and T_0 were determined from the linear extrapolation of reciprocal dependence of the dielectric permittivity versus temperature (Fig. 8b), above Curie temperature. The obtained values are $T_0 = 87\ ^oC$ and $C = 3.329 \cdot 10^4$ K. Curie-Weiss constant is reflection of the microstructure. Small grained, dense structure shows higher C values, while porous one mostly displays smaller C. Fine-grained barium titanate ceramics exhibit C with an order of magnitude 10^5 [43]. The Curie-Weiss constant for our sample has value for one order of magnitude smaller, indicating the presence of porous microstructure, which is in good correlation with the SEM micrograph.

4. Conclusion

In this paper the new approach for the preparation of tetragonal, nanocrystalline $BaTiO_3$, was shown. Obtaining tetragonal barium titanate as a major phase at temperature significantly below 1000 ^oC by using this method was achieved. Sintering temperature was decreased, comparing to other synthesis methods. Raman measurement showed that sintered sample still has small amount of the secondary phases ($BaTi_2O_5$, Ba_2TiO_4, TiO_2) indicating that reaction hasn't completed. Dielectric parameters confirm significant influence of density on ε_r and loss tangent. Low achieved density suggests that the sintering temperature should be increased or dwell time prolonged, toward improving dielectric parameters. Also, ordered crystal structure was demonstrated by Raman and dielectric measurement. It was proven that prepared $BaTiO_3$ follow Curie-Weiss low and characteristic parameters were determined.

Although obtained material does not possess excellent properties, obtained results and considerable improved experimental conditions – decreased temperature of reaction, adequate precursor, etc. may affect further development in the field, as well as the rational design of new barium titanate with desired properties.

Acknowledgments

Funds for the realization of this work are provided by the Ministry of Education, Science and Technological Development of the Republic of Serbia, Agreement on realization and financing of scientific research work of the Institute of Technical Sciences of SASA in 2020 (Record number: 451-03-68 / 2020-14 / 200175) .

5. References

1. D. A. Kosanović, V. A. Blagojević, N. J. Labus, N. B. Tadić, V. B. Pavlović, M. M. Ristić, Effect of Chemical Composition on Microstructural Properties and Sintering Kinetics of (Ba,Sr)TiO_3 Powders, Sci. Sint. 50 (2018) 29-38.
2. A. A. Komlev, I. I. Bachigina, A. V. Pokrovskii, M. A. Ishchenko, E. F. Vilezhaninov, Formation of Barium Titanate in Combustion of heterogeneous Condensed Systems, Russ. J. Appl. Chem. 87 (201) 1210-1216.
3. W. Chen, H. Hao, Y. Yang, C. Chen, M. Appiah, Z. Yao, M. Cao, Z. Yu, H. Liu, Dielectric properties and impedance analysis of $BaTiO_3$-based ceramics with core-shell structure, Ceram. Inter. 43 (2017) 8449-8458.
4. R. Jacob, H. G. Nair, J. Isac, Impedance spectroscopy and dielectric studies of nanocrystalline iron doped barium strontium titanate ceramics, Process. and Appl. of Ceram. 9 [2] (2015) 73-79.
5. E. A. Zereffa, T. A. Seghne, Sintering Temperature, Microstructures and Electrical Properties of $(Na_{1/2}Bi_{1/2})_{0.94}Ba_{0.06}Ti_{0.97}(Mg_{1/3}Nb_{2/3})_{0.03}O_3$ Ferroelectric Ceramic, Sci. Sint. 50 (2018) 245-253.
6. D. Hu, K. Mori, X. Kong, K. Shinagawa, S. Wada, Q. Feng, Fabrication of [1 0 0]-oriented bismuth sodium titanate ceramics with small grain size and high density for piezoelectric materials, J. Europ. Ceram. Soc. 34 (2014) 1169-1180.
7. J. Li, K. Inukai, A. Tsuruta, Y. Takahashi, W. Shin, Synthesis of highly disperse tetragonal $BaTiO_3$ nanoparticles with core–shell by a hydrothermal method, J. As. Ceram. Soc. 5 (2017) 444-451.
8. B. Jiang, J. Iocozzia, L. Zhao, H. Zhang, Y.-W. Harn, Y. Chen, Z. Lin, Barium titanate at the nanoscale: controlled synthesis and dielectric and ferroelectric properties, Chem. Soc. Rev. 48 (2019) 1194-1228.
9. M. T. Buscaglia, M. Bassoli, V. Buscaglia, and R. Alessio, Solid-State Synthesis of Ultrafine $BaTiO_3$ Powders Form Nanocrystalline $BaCO_3$ and TiO_2, J. Am. Ceram. Soc. 88 (2005) 2374-2379.
10. V. P. Pavlović, B. Stojanović, V. B. Pavlović, Z. Marinković-Stanojević, Lj. Živković, M. Ristić, Synthesis of $BaTiO_3$ From a Mechanically Activated $BaCO_3$–TiO_2 System, Sci. Sint. 40 (2008) 21-26.
11. A. Maghtada, A. H. Moghadam, R. Ashiri, Tetragonality enhancement in $BaTiO_3$ by mechanical activation of the starting $BaCO_3$ and TiO_2 powders: characterization of the contribution of the mechanical activation and postmilling calcination phenomena, Int. J. Appl. Ceram. Technol. 15 (2018) 1518-1531.
12. V. P. Pavlović, B. D. Stojanović, V. B. Pavlović, Lj. Živković, M. M. Ristić, Low temperature sintering of mechanically activated $BaCO_3$-TiO_2, Sci. Sint. 34 (2002) 73-77.
13. Md. J. Ansaree, S. Upadhyay, Thermal analysis of formation of nano-crystalline $BaTiO_3$ using $Ba(NO_3)_2$ and TiO_2, Proc. and App. of Ceram. 9 [4] (2015) 181-185.
14. S. Kazaoui, J. Ravez, Dielectric relaxation in $Ba(Ti_{0.8}Zr_{0.2})O_3$ ceramics prepared fromsol-gel and solid state reaction powders, J. Mater. Sci. 28 (1993) 1211-1219.
15. J. Bera, D. Sarkar, Formation of $BaTiO_3$ from barium oxalate and TiO_2, J. Electroceram. 11 (2003) 131-137.
16. H. S. Potdar, S. B. Deshpande, A. S. Deshpande, Y. B.Khollam, A. J. Patil, S. D. Pradhan, S. K. Date, Simplified chemical route for the synthesis of barium titanyl oxalate (BTO), Inter. J. Inorg. Mater. 3 (2001), 613-623.
17. C. Coudaren, T. Bataille, J.P. Auffredic, D. Louer, Synthesis, structure determination from powder diffraction data and thermal behaviour of titanium(IV) oxalate $[Ti_2O_3(H_2O)_2](C_2O_4)\cdot H_2O$, Solid State Sciences, 5 (2003) 175-182.
18. R.W. Cheary, A. Coelho, Fundamental parameters approach to X-ray line-profile fitting, J. Appl. Crystallogr., 25 (1992) 109-121.

19. M. H. Frey, D. A. Payne, Grain-size effect on structure and phase transformations for barium titanate, Phys. Rev. B 54 (1996) 3158-3168.
20. Y. I. Kim, J. K. Jung, and K. S. Ryu, Structural Study of Nano $BaTiO_3$ Powder by Rietveld Refinement, Mater. Res. Bull. 39 [7–8] (2004) 1045-1053.
21. V. P. Pavlović, M. V. Nikolić, V. B. Pavlović, J. Blanuša, S. Stevanović, V. V. Mitić, M.Šćepanović, B. Vlahović, Raman Responses in Mechanically Activated $BaTiO_3$, J. Am. Ceram. Soc. 97 (2014) 601-608.
22. W. E. Rhine, R. B. Hallock, W. M. Davis, W. Wong-Ng, Synthesis and Crystal Structure of Barium Titanyl Oxalate, $BaTi(O)(C_2O_4)_2{\cdot}5H_2O$: A Molecular Precursor for $BaTiO_3$, Chem. Mater. 4 (1992) 1208-1216.
23. M. M. Vijatović, J. D. Bobić, B. D. Stojanović, History and Challenges of Barium Titanate: Part II, Sci. of Sint. 40 (2008) 235-244.
24. J. Q. Qi, T. Peng, Y. M. Hu, L. Sun, Y. Wang, W. P. Chen, L. T. Li, C. W. Nan, H. L. W. Chan, Direct synthesis of ultrafine tetragonal $BaTiO_3$, nanoparticles at room temperature, Nanoscale Res. Lett. 6 (2011) 466-469.
25. P. C. Ricci, C. M. Carbonaro, L. Stagi, M. Salis, A. Casu, S. Enzo, F. Delogu, Anatasee-to-Rutile Phase Transition in TiO_2 Nanoparticles Irradiated by Visible Light, J. Phys. Chem. C 117 (2013) 7850-7857.
26. Y. Jing-Xin, F. Min, J. Guang-Fu, C. Xiang-Rong, Phase transition and thermodynamic properties of TiO_2 from first-principles calculations, Chinese Phys. B 18 (2009) 269-274.
27. B. N. Cardoso, E. C. Kohlrausch, M. T. Laranjo, E. V. Benvenutti, N. M. Balzaretti, L. T. Arenas, M. J. L. Santos, T. M. H. Costa, Tuning Anatase-Rutile Phase Transition Temperature: TiO_2/SiO_2 Nanoparticles Applied in Dye-Sensitized Solar Cells, International Journal of Photoenergy, 2019, Article ID 7183978, 9 pages, 2019. https://doi.org/10.1155/2019/7183978.
28. D. A. H. Hanaor, C. C. Sorrell, Review of the anatasee to rutile phase transformation, J. Mater. Sci. 46 (2011) 855-874.
29. S. Nie, Y. Liu, Q. Liu, M. Wang, H. Wang, Phase transitions and thermal expansion of $BaCO_3$ and $SrCO_3$ up to 1413K, Eur. J. Mineral. 29 (2017) 433-443.
30. C. Teichmann, J. Töpfer, Low-temperature sintering of $BaTiO_3$ positive temperature coefficient of resistivity (PTCR) ceramics, J. of Mater. Sci.: Mater. in Electronics 29 (2018) 17881-17886.
31. H. Naghib-zadeh, C. Glitzky, I. Dörfel, T. Rabe, Low temperature sintering of barium titanate ceramics assistedby addition of lithium fluoride-containing sintering additives, J. of the Eur. Ceram. Soc. 30 (2010) 81-86.
32. S. Filipović, V. P. Petrović, M. Mitrić, S. Lević, N. Mitrović, A. Maričić, B. Vlahović, V. B. Pavlović, Synthesis and characterization of $BaTiO_3/\alpha$-Fe_2O_3 core/shell structure, J. Adv. Ceram. 8(1) (2019) 133-147.
33. R. Naik, J. J. Nazarko, C.S. Flattery, U. D. Venkateswaran, V. M. Naik, M.S. Mohammed, G. W. Auner, J. V. Mantese, N. W. Schubring, A. L. Micheli, A. B. Catalan, Temperature dependence of the Raman spectra of polycrystalline Ba1–*x*Si*x*TiO_3, Phys. Rev. *B* 61 (2000) 11367-11372.
34. M. B. Smith, K. Page, T. Siegrist, P. L. Redmond, E. C. Walter, R. Seshadri, L. E. Brus, M. L. Steigerwald, Crystal Structure and the Paraelectric-to-Ferroelectric Phase Transition of Nanoscale $BaTiO_3$, J. Am. Chem. Soc. 130 (2008) 6955-6963.
35. T. C. Huang, M. T. Wang, H. S. Sheu, W.F. Hsieh, Size-dependent lattice dynamics of barium titanate nanoparticles, J. Phys.: Condens. Matter 19 (2007) 476212-12.
36. D. A. H. Hanaor, C.C. Sorrell, Review of the anatase to rutile phase transformation, J Mater Sci (2011) 46:855-874.
37. J. Peng, C. Wang, L. Li, Q. Shen, L. M. Zhang, Synthesis of Single-phased $BaTi_2O_5$ Powders by Arc-melting, Adv. Mater. Res. 279 (2011) 44-48.

38. S. Marković, M. Lukić, S. D. Škapin, B. Stojanović, D. Uskoković, Designing, fabrication and characterization of nanostructured functionally graded HAp/BCP ceramics, Ceram. Int. 41 (2015) 2654-2667.
39. K.-H. Felgnera, T. Mullerb, H. T. Langhammera, H.-P. Abicht, On the formation of $BaTiO_3$ from $BaCO_3$ and TiO_2 by microwave and conventional heating, Mater. Lett. 58 (2004) 1943-1947.
40. S. Filipović, N. Obradović, S. Marković, M. Mitrić, I. Balać, A. Đordević, V. Pavlović, The effect of ball milling on properties of sintered manganese-doped alumina, Ad. Powder Tech. 30 (2019) 2533-2540.
41. A. R. Đorđević, D. I. Olćan, N. Obradović, V. Paunović, S. Filipović, V. B. Pavlović, Electrical Properties of Magnesium Titanate Ceramics Post-Sintered by Hot Isostatic Pressing, Sci. Sint. 49 (2017) 373-380.
42. A. Kholodkova, M. Danchevskaya, N. Popova, L. Pavlyukova, A. Fionov, Preparation and dielectric properties of thermo-vaporous $BaTiO_3$ ceramics, Mater. and tech. 49 (2015) 3, 447-451.
43. V. Paunović, V. V. Mitić, Lj. Kocić, Dielectric characteristics of donor-acceptor modified $BaTiO_3$ ceramics, Ceram. Inter. 42 (2016) 11692-11699.
44. Y. Li, Z. Liao, F. Fang, X. Wang, L. Li, J. Zhu, Significant increase of Curie temperature in nano-scale $BaTiO_3$, Appl. Phys. Lett. 105, (2014) 182901-4.
45. P. V. Balachandran, D. Xue, T. Lookman1, Structure–Curie temperature relationships in $BaTiO_3$-based ferroelectric perovskites: Anomalous behavior of (Ba,Cd)TiO_3 from DFT, statistical inference, and experiments, Phys. Rev. B 93 (2016) 144111-12.
46. B. A. Marinković, B. D. Stojanović, V. B. Pavlović, V. P. Pavlović, M. M. Ristić, Correlation of Microstructure and Dielectrical Properties of $BaTiO_3$ Sintered from Mechanically Activated Powders, Mater. Struc. 6 (1999) 96-99.
47. Y. Yan, C. Ning, Z. Jin, H. Qin, W. Luo, G. Liu, The dielectric properties and microstructure of $BaTiO_3$ ceramics with ZnO-Nb_2O_5 composite addition, J. Alloy. Comp. 646 (2015) 748-752.

Сажетак: *Баријум титанат ($BaTiO_3$) привлачи значајну научну и технолошку пажњу захваљујући његовим добрим диелектричним електро-механичким својствима. Иако $BaTiO_3$ је један од најчешће коришћених фероелектричних материјала, потреба за проналажењем новог или унапређивање постојећих начина синтезе овог материјала, још увек постоји. У овом радуприказана је нова, лагана метода синтезе тетрагоналног $BaTiO_3$ из баријум нитрата и титанијум оксалата. Морфологија синтетисаног и накнадно синтерованог баријум титаната је испитана скенирајућом електронском микроскопијом. Расподела величина честица синтетисљаног праха је праћена дифракцијом ласерских зрака. Фазни састав и динамика решетке су испитиване методама дифракције ренгенских зрака и Рамановом спектроскопијом. На крају, промене у диелектричним параметрим су измерене у температурском интервалу од 30 до 180 ^oC, Киријева температура је детектована на 130 ^oC.*

Кључне речи*: нанокристални $BaTiO_3$, синтеза сагоревањем, рендгеноструктурна анализа, раманска спектроскопија, диелектрична својства.*